Apoptosis (2023) 28:210–221
https://doi.org/10.1007/s10495-022-01788-z

Upregulation of miR-29b-3p alleviates coronary microembolization-induced myocardial injury via regulating BMF and GSK-3β

Zhenbai Qin[1] · Xiantao Wang[1] · You Zhou[1] · Jing Zheng[1] · Hongqing Li[1] · Lang Li[1]

Accepted: 24 October 2022 / Published online: 31 October 2022

Abstract
Coronary microembolization (CME) is an intractable complication results from acute coronary syndrome. CME-induced myocardial apoptosis was associated with progressive cardiac contractile dysfunction. miR-29b-3p has been reported implicated in variety cardiovascular diseases, but its function in CME-induced myocardial injury is yet unknown. Herein, a rat model of CME was established by injecting microspheres into the left ventricle and found that the expression level of miR-29b-3p was markedly decreased in the CME rat heart tissues. By using echocardiography, CD31 immunohistochemistry staining, hematoxylin basic fuchsin picric acid (HBFP) staining, TUNEL staining, and western blotting analysis after CME, it was found that upregulating miR-29b-3p improved cardiac dysfunction, promoted angiogenesis, decreased myocardial microinfarct area, and inhibited myocardial apoptosis. Additionally, miR-29b-3p inhibition can reverse the protective benefits of miR-29b-3p overexpression. Mechanistically, the target genes of miR-29b-3p were identified as glycogen synthase kinase 3 (GSK-3β) and Bcl-2 modifying factor (BMF) by bioinformatics analysis and luciferase reporter experiment. Overall, our findings imply that induction of miR-29b-3p, which negatively regulates GSK-3β and BMF expression, attenuates CME-induced myocardial injury, suggesting a novel potential therapeutic target for cardioprotective after CME.

Keywords Coronary microembolization · miR-29b-3p · GSK-3β · BMF

Introduction

Coronary microembolization (CME), which is caused by the spontaneous erosion or rupture of an epicardial coronary atherosclerotic plaque, has emerged as a serious clinical issue with the increased use of elective and primary percutaneous coronary intervention (PCI) [1, 2]. As a predictor of acute coronary syndrome (ACS) patient prognosis independent of and in addition to infarct area size, CME was linked with coronary no-reflow and slow-flow phenomena [3–5]. According to studies, CME frequently results in an inflammatory response and myocardial apoptosis, both of which advance myocardial contractile dysfunction [6, 7]. Therefore, understanding the mechanism underlying CME-induced myocardial damage is essential to both treating and preventing CME.

Recently, research on cardiovascular disease has increasingly focus on non-coding RNAs and their effects in regulating gene expression at the transcriptional and post-transcriptional levels. MicroRNAs (miRNAs) are small non-coding endogenous RNAs and about 18–24 nucleotides in length that bind to the target sites in the 3′-untranslated region (3′-UTR) of messenger RNA to regulate posttranscriptional gene expression [8]. miRNAs have conserved interactions with most human mRNAs and abnormal expression of miRNAs is implicated in many human diseases, particularly cardiovascular disease (CVD) [9, 10]. The miR-29 family are highly conserved and consists of miR-29a, miR-29b and miR-29c. Several studies have demonstrated that miR-29 s largely involves in the pathogenesis of CVD, including cell proliferation, atherosclerosis, myocardial ischemia/reperfusion injury, heart failure, etc. [11]. By using miRNA specific probes van Rooij reported that all three isoforms of miR-29 were significantly down-regulated in the areas bordering the infarcted myocardium in mice and miR-29b in human hearts

✉ Lang Li
drlilang1968@126.com

[1] Department of Cardiology, The First Affiliated Hospital of Guangxi Medical University, No. 6 Shuangyong Road, Qingxiu District, Nannig 530021, Guangxi, China

[12]. miR-29b-3p was highly expression in heart tissue, and it is striking decrease in the plasma of congestive heart failure patients, indicating a high chance of participation of miR-29b-3p in cardiac dysfunction [13]. Cai showed that overexpression of miR-29b-3p inhibits hypoxia-induced cardiomyocytes apoptosis via suppressing TRAF5 expression [14]. However, whether miR-29b-3p expression is related to CME-induced myocardial injury and how it affected myocardial apoptosis remains largely unknown.

In this study, we established a rat model of CME by injecting polyethylene microspheres into the left ventricle. Our results showed that miR-29b-3p was remarkably down-regulated post-CME, overexpression of miR-29b-3p by transfecting miRNA mimics before CME modeling inhibited CME-induced myocardial apoptosis, promoted angiogenesis and improved cardiac function, while transfecting with miRNA inhibitor had opposite effects. Additionally, we confirmed GSK-3β and BMF as direct target genes of miR-29b-3p. Collectively, we identified miR-29b-3p as an antiapoptotic miRNA that is down-regulated in the myocardium after CME. Overexpression of miR-29b-3p could be a protective strategy to inhibit myocardial apoptosis and improve cardiac function following CME.

Materials and methods

Animal model establishment

SD rats were purchased from the Experimental Animal Center of Guangxi Medical University. The animals received normal rat chow and water under a 12-h light/dark cycle at 23 ± 2 °C. The study protocol rats CME model was established as previous described [7]. Briefly, pentobarbitone sodium (40 mg/kg) was administered intraperitoneally to anesthetize the rats. An animal ventilator (70 breaths per minute, 20 ml tidal volume) was then connected to help the animals breathe. Following shaving of the rat's chest skin, routine disinfection, and installation of sterile surgical cloths, the second to fourth intercostal gaps were cut open until the heart was clearly visible. Next, the pericardium was removed, the ascending aorta was separated, and an appropriate animal hemostatic clip was used to clamp the ascending aorta for 12 s while a total of 4500 polyethylene microspheres (Polybead Microspheres, diameter 45 μm; Polysciences Inc., USA) were injected into the left ventricle. Rats in the Sham group received 0.15 ml normal saline along with similar treatment. All animal experiments were approved by the Animal Research Ethics Committee of Guangxi Medical University and in accordance with the National Institutes of Health Guide for the Care and Use of Laboratory Animals.

Adeno-associated virus transfection and experimental animal grouping

To uncover the relation between miR-29b-3p expression level and CME, twenty rats were randomized divided into sham and CME group (n = 10 per group). For miR-29b-3p regulation study, we transfected rats with recombinant adeno-associated virus serotype 9 (AAV, 1×10 [12] vector genomes (vg)/per rat) through tail vain injection 28 days before operation. Briefly, fifty rats were randomly divided into five groups (n = 10 per group): sham, CME, CME + AAV-miR-29b-3p negative control (miR-NC), CME + AAV-miR-29b-3p mimics (miR-mimic) and CME + AAV-miR-29b-3p inhibitors (miR-inhibitor). AAV used in this study was designed and constructed by Shanghai Genechem Co.,Ltd. (Shanghai, China).

Echocardiography

Our previous study discovered that rat cardiac function reach the poorest level at 12 h after CME operation [15]. Therefore, we detected rats cardiac function at 12 h post-CME in the present study. Briefly, rats received pentobarbitone sodium (30–40 mg/kg) intraperitoneally for anesthetic, and then left ventricular end-diastolic diameter (LVEDd), left ventricular fractional shortening (LVFS), left ventricular end-systolic diameter (LVEDs), and left ventricular ejection fraction (LVEF) were assessed by using an animal specific ultrasound instrument (Esaote, MyLabSix, Italy) according to the manufacturer's instruction. The results were average from three cardiac cycle, and measurement was performed by specialist blinded to the study.

Tissue sampling and treatment

After cardiac function examination, rats received pentobarbitone sodium (60 mg/kg) intraperitoneally. Blood sample were collect from abdominal aorta for ELISA essay detection. After that, heart tissue was extracted and rinsed with cool normal saline, and then cut into apex and bottom part. The apex part was put into liquid nitrogen immediately for Western blot and quantitative real-time polymerase chain reaction (qRT-PCR) analysis. The bottom part was fixed in 4% paraformaldehyde, embedded into paraffin, and serially sliced into 4 μm sections for histological analysis.

Myocardial injury and oxidative stress measurement

Rats serum c-troponin I (cTnI) and creatine kinase MB isoenzyme (CK-MB) were detected by using a rat cTnI ELISA kit (Bio-Swamp RA20107, Wuhan, China) and CK-MB

ELISA kit (Bio-Swamp RA20038, Wuhan, China) according to the manufacturer's instructions. For myocardium oxidative stress analyses, we measured serum SOD, CAT and MDA concentrations by using SOD assay kit, MDA assay kit (Nanjing Jiancheng Bioengineering Institute, Nanjing, China) and CAT assay kit (Solarbio, Beijing, China) according to the manufacturer's instruction.

Histological analysis

The size of the myocardial microinfarct and changes in the morphology of the tissues were identified using HE staining and HBFP staining, respectively. Hematoxylin basic fuchsin picric acid (HBFP) staining, which stains normal cardiomyocyte cytoplasm yellow and nuclei blue while staining ischemic myocardium and erythrocytes red, can detect early myocardial ischemia. Five randomly fields of each section were observed and microinfarct size calculated as: infarct area/ total observed area [7]. Myocardial apoptosis was detected by TUNEL staining, apoptotic cells nuclei were stained red and blue nuclei represents normal. Apoptosis index was calculated as: apoptotic cells/ total cells. The rabbit detection kit for anti-rat CD31 (1:1000; ab182981, abcam) was applied to evaluate myocardial neovascularization. To calculate microvessels density, entire slices were scanned carefully with a lower magnification (×40) optical microscope to find the areas of high vessel density as "hot spots" and vessels in the hot spot area stained brown by anti-CD31 antibody was counted under a light microscope (×200). Three hot spot areas were selected for further evaluation and single endothelial cell or cluster of cells stained brown that were separated from adjacent vessels was considered an individual vessel [16]. All above study were performed according to the manufacturer's instruction and experiment data were analyzed via Image-Pro Plus 6.0 software (Media Cybernetics, Sliver Springs, MD, USA).

Target gene prediction and dual-luciferase reporter assay

The target of miR-29b-3p was predicted by using TargetScan version 7.2 (www.targetscan.org/vert_72/) and miRBD (http://mirdb.org/). BMF and GSK-3β associated with apoptosis and angiogenesis were identified to contain putative binding sites of miR-29b-3p. To confirm miR-29b-3p can direct regulate BMF and GSK-3β expression, we performed luciferase reporter assay. BMF and GSK-3β 3′UTR containing the wild type binding sequences of miR-29b-3p (BMF 3'UTR-wt, GSK-3β 3′UTR-wt, respectively) and corresponding mutant constructs (BMF 3′UTR-mut, GSK-3β 3′UTR-mut, respectively) were design and synthesized by Hanbio Biotechnology Shanghai, China. Briefly, these fragments were amplified into pSI-Check2 vector (Hanbio Biotechnology) and then co-transfected into HEK-293 T cells together with miR-29b-3p mimics or miR-29b-3p negative control using Lipofectamine 2000 (Invitrogen). After 48 h transfection, the luciferase activity was examined with a Dual Luciferase System (Promega) and normalized to Renilla luciferase activity.

Quantitative real-time PCR

Total RNA was extracted from heart tissues by the TRIZOL method (Invitrogen) and concentration quantified by NanoDrop 2000 (Thermo Fisher Scientific Inc., USA). After that, mRNA and miRNA reverse transcribed was conducted using a PrimeScript RT Reagent kit and Mir-X™ miRNA First-Strand Synthesis Kit (Takara, Dalian, China), respectively. qPCR was performed using a TB Green Premix Ex Taq II kit on ABI PRISM 7500 Fast Real-time PCR instrument (Applied BioSystems, USA). Forward primer sequence for miR-29b-3p: 5′-CGCCCATTTGAAATCAGTGTTA-3′; and optimized miRNA reverse primer and U6 primer from Takara were used. Gene expression levels were normalized to U6 expression by using $2^{-\Delta\Delta Ct}$ method.

Western blot analysis

Cardiac proteins were extracted using RIPA lysis (Beyotime, China) buffer and quantified by using BCA assay kit (Beyotime, China) according to the manufacturer's manual. After quantification, 25 μg of protein was separated by 10 ~ 12% sodium dodecyl sulfate polyacrylamide gel electrophoresis (SDS-PAGE), and transferred onto PVDF membranes (Millipore). Subsequently, the membranes were block with 5% skim milk 1 h at room temperature, and then incubated into primary antibodies against BMF (GTX59683, GeneTex), GSK-3β(D5C5Z, CST), Bcl-2(sc-7382, Santa Cruz), Cleaved-caspase-3 (9661S, CST), Bax (ab32503, abcam),Cleaved-caspase-9 (9508S, CST), GST (2625 T, CST), NQO1(ab80588, abcam) and GAPDH (ab181602, abcam) at 4 ℃ overnight, followed by probed with indicated secondary antibody conjugated with horseradish peroxidase for 1 h at room temperature. All Western blots were detected by enhanced chemiluminescence reagents (Pierce, Rockford, IL, USA) and the gray value of protein bands were analyzed using Image J software.

Statistical analysis

All results were analyzed with SPSS 17.0 software and presented as the mean ± standard deviation (SD). Two groups comparison were made by Student's t-test. One-way analysis of variance (ANOVA) followed by Bonferroni post hoc test

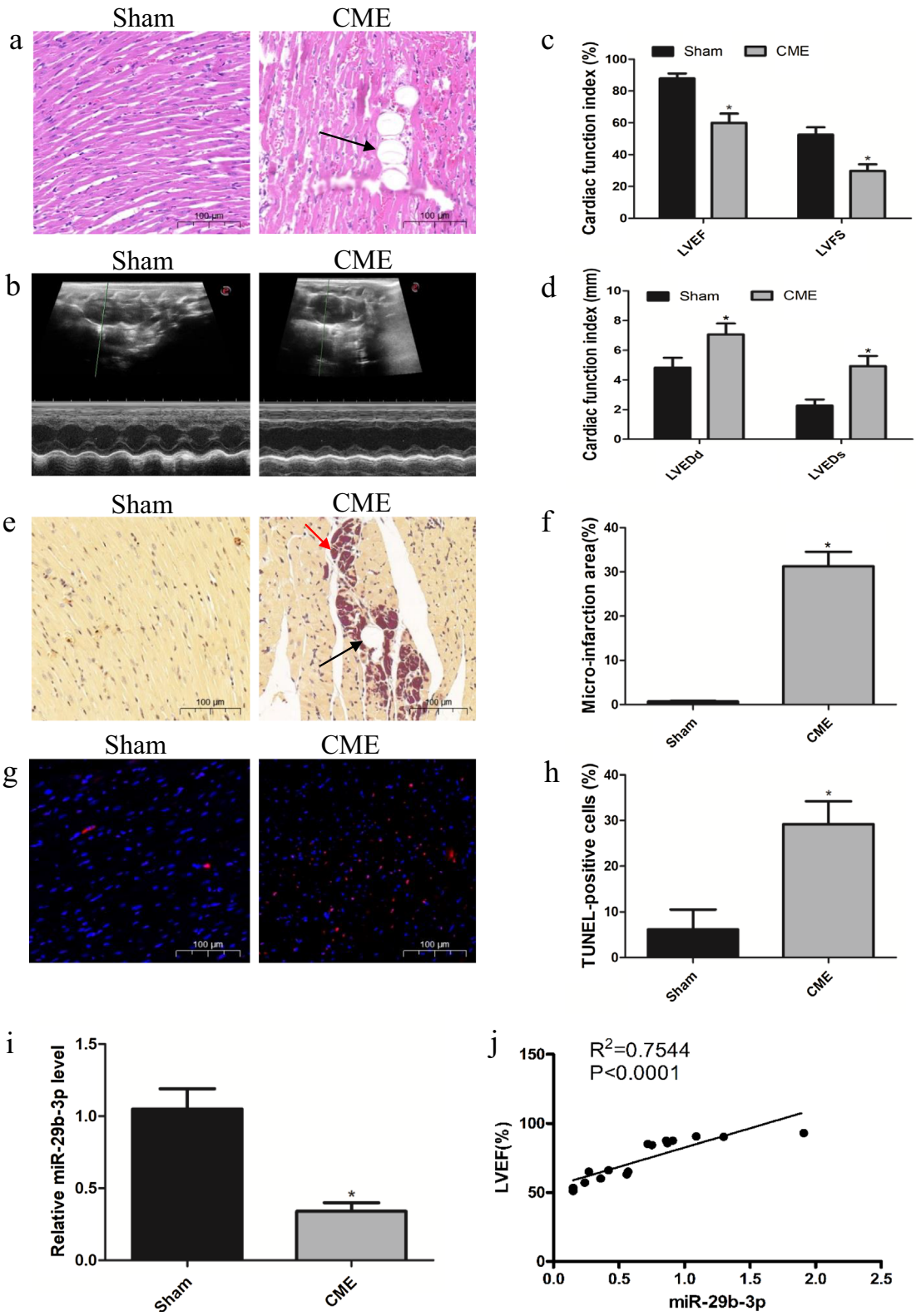
a
Sham
CME
100 μm
b
Sham
CME
c
Sham
CME
Cardiac function index (%)
LVEF
LVFS
d
Cardiac function index (mm)
LVEDd
LVEDs
e
Sham
CME
100 μm
f
Micro-infarction area(%)
Sham
CME
g
Sham
CME
100 μm
h
TUNEL-positive cells (%)
Sham
CME
i
Relative miR-29b-3p level
Sham
CME
j
R2=0.7544
P<0.0001
LVEF(%)
miR-29b-3p

◂**Fig. 1** miR-29b-3p is down-regulated 12 h after CME and induces myocardial apoptosis. **a** Representative pictures of HE staining in Sham and CME group. n = 6 per group, scale bar = 100 μm. The black arrow indicates microspheres. **b** Cardiac function analyzed by echocardiography 12 h after CME or Sham surgery. **c** and **d** Quantitative analysis of LVEF, LVFS, LVEDd and LVEDs. n = 8 per group; *$p < 0.05$ versus Sham. **e** Representative images of HBFP-stained of heart sections. n = 3 per group, scale bar = 100 μm. The red arrow indicates micro-infarct focus, and black arrow indicates microspheres. **f** Quantitative analysis of the micro-infarct areas in heart sections. n = 3 per group; *$p < 0.05$ versus Sham. **g** Representative images of TUNEL staining in Sham and CME group. n = 3 per group, scale bar = 100 μm. **h** Quantification of percentage of TUNEL-positive cardiomyocytes in g. n = 3 per group; *$p < 0.05$ versus Sham. **i** qPCR of miR-29b-3p on RNA extracted from myocardium 12 h after Sham or CME operation. n = 8 per group; *$p < 0.05$ versus Sham. **j** The correlation between miR-29b-3p level and LVEF. n = 8, $R.^2 = 0.7544$, $p < 0.0001$

was performed to compare differences between multi-groups. A value of $P < 0.05$ was considered statistically significant.

Results

CME induces myocardial injury and downregulates miR-29b-3p in rats

In an effort to identify whether miR-29b-3p dysregulated within 12 h after CME and investigate the relation between miR-29b-3p expression level and CME-induced cardiac injury, a rat model of CME was established by injecting polyethylene microspheres into the left ventricle. We found that cardiac function were significantly decreased in CME group compared to the sham group (Fig. 1 b through 1d). HE staining results showed that CME model was successful built, and myocardial morphology was severely damage as indicates in myocardium degeneration, necrosis, and inflammatory cell infiltration (Fig. 1a). HPFB staining revealed that there was significant microinfarction foci in the CME group, and no infarct sign in the sham group (Fig. 1e, f). TUNEL staining showed that a great number of TUNEL-positive nuclei were observed in the CME group compared to the sham group (Fig. 1g, h). qPCR data revealed that miR-29b-3p expression level was significantly decreased post-CME compared to the sham group (Fig. 1i). What's more, the correlation analysis between miR-29b-3p expression level and LVEF showed a positive correlation result (Fig. 1j). These preliminary results suggested that miR-29b-3p might play a key role in CME-induced myocardial injury and apoptosis.

miR-29b-3p suppresses myocardial apoptosis and improves cardiac function

Apoptotic signals are activated in response to microcirculation dysfunction in the heart. Therefore, we guessed that myocardial apoptosis post-CME may be related to the decreased expression levels of miR-29b-3p. Subsequently, we injected miR-29b-3p mimics to overexpression miR-29b-3p through tail vein in rats by using a Lipofectamine-mediated transfection method. qPCR and immunofluorescence staining were performed to validate the transfection efficiency. As shown in Fig. 2a and b, strong green fluorescence and high expression levels of miR-29b-3p in the heart altogether revealed miR-29b-3p mimics efficient uptake.

To validate whether upregulation miR-29b-3p can suppress myocardial apoptosis in vivo, we performed TUNEL staining, and Western blot analysis of apoptosis-related protein expression levels. The percentage of TUNEL-positive cardiomyocytes was significantly lower in the miR-mimic group than CME and miR-NC group (Fig. 2c, d). Moreover, miR-29b-3p mimic treatment markedly suppressed pro-apoptotic protein Bax, Cleaved-caspase3 and Cleaved-caspase9 expression, while increased anti-apoptosis protein Bcl-2 expression (Fig. 2j, k). We speculated that a reduction of cardiomyocytes apoptosis by miR-29b-3p would translate into reduced cardiac dysfunction. Echocardiography results revealed that treatment with miR-29b-3p mimic significantly improved heart function, as LVEF and LVFS were remarkably elevated, while LVEDd and LVEDs were decreased, compared to the CME and miR-NC groups (Fig. 2g and Table 1). Consistent with the improvement of heart function, myocardial microinfarct sizes and serum cTnI and CK-MB concentrations were significantly decreased in miR-29b-3p recipient rats (Fig. 2e, f and h, i). These results suggested that miR-29b-3p mimic exert cardioprotective role against CME-induced myocardial injury partially through inhibits myocardial apoptosis.

miR-29b-3p improved myocardial antioxidative ability following CME

After CME, an imbalance between oxidants and antioxidants can result in a buildup of oxidants in the myocardium, which causes cardiomyocytes to undergo apoptosis and results in oxidative stress. To determine whether overexpression of miR-29b-3p could inhibit the degree of CME-induced oxidative stress, we detected serum superoxide dismutase (SOD), malondialdehyde (MDA) and catalase (CAT) contents. As shown in Fig. 3a through 3c, SOD and CAT were significantly decreased together with MDA content increased in the CME and miR-NC groups compared with the sham group. Interestingly, rat treated with miR-29b-3p had an elevation in SOD and CAT activity, while MDA content was remarkably decreased. In addition, Western blotting results demonstrated that the main detoxification system protein for cells to resist oxidative damage NQO1 and GST were significant elevated in miR-mimic group compared to the miR-NC and CME groups (Fig. 3d, e). These results demonstrated that miR-29b-3p upregulation promoted myocardial antioxidant ability after CME.

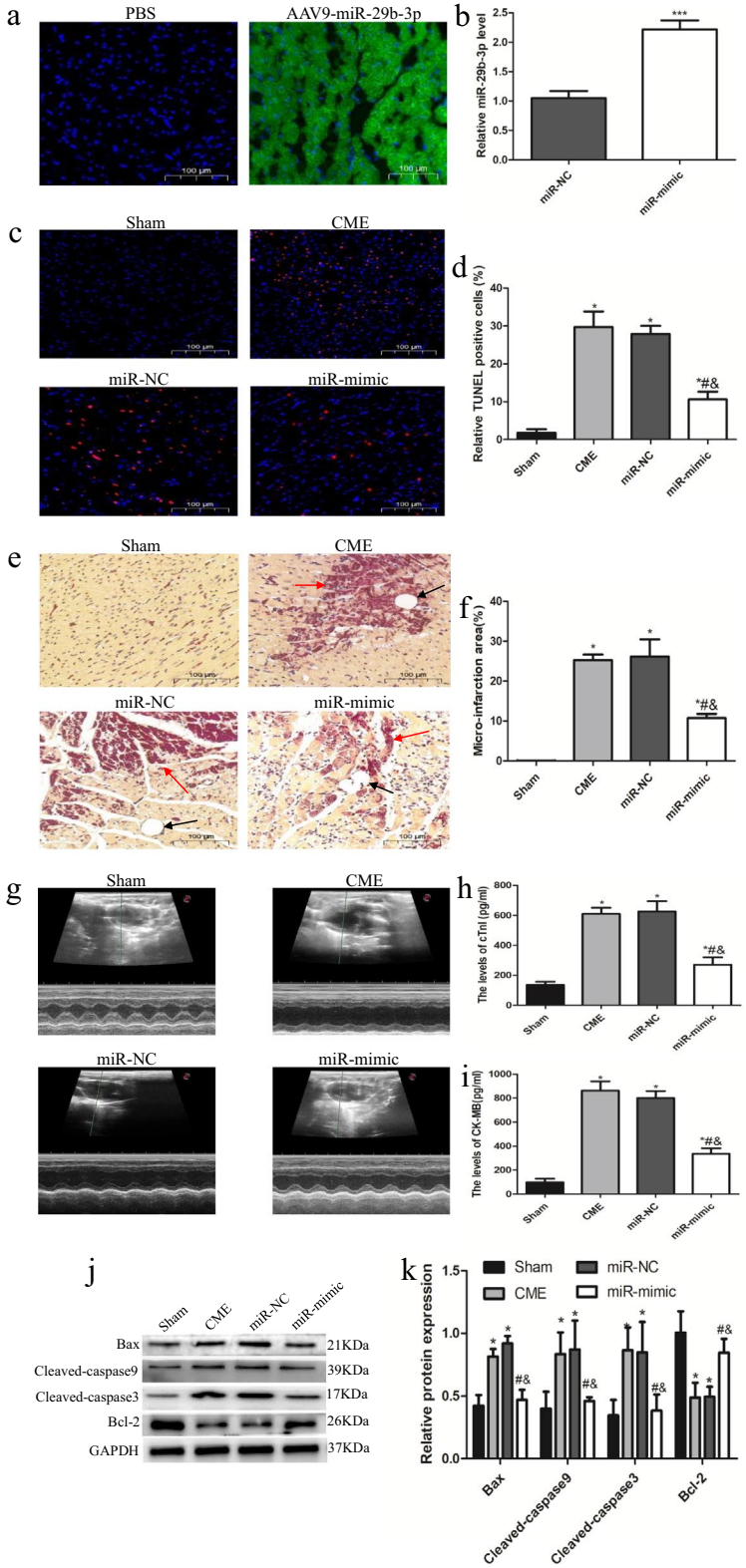

Fig. 2 In vivo delivery of miR-29b-3p inhibits myocardial apoptosis and improves cardiac function. **a** GFP/DAPI double-staining in hearts 28 days after injection of AAV9-miR-29b-3p or PBS. n = 3 per group, scale bar = 100 μm. Blue indicates nucleus stained, and green fluorescence represents GFP-AAV-9-miR-29b-3p. **b** Relative miR29b-3p expression level was increased in myocardium after AAV9-miR-29b-3p transfection. n = 10 per group, ***$p < 0.05$ versus miR-NC. **c** TUNEL staining of heart Sects. 12 h after surgery. DAPI was used for nuclear staining, and TUNEL-positive nuclei were red stained. n = 5 per group, scale bar = 100 μm. **d** Percentage of TUNEL positive cardiomyocytes of hearts. n = 5 per group; *$p < 0.05$ vs Sham, #$p < 0.05$ vs CME, &$p < 0.05$ vs miR-NC. **e** HBFP staining on heart section of Sham, CME, miR-NC and miR-mimic groups. n = 5 per group, scale bar = 100 μm. The black arrow indicates microspheres, red arrow shows microinfarct foci. **f** Quantitative analysis of the microinfarct areas in heart sections. n = 5 per group; *$p < 0.05$ vs Sham, #$p < 0.05$ vs CME, &$p < 0.05$ vs miR-NC. **g** Cardiac function analyzed by echocardiography. n = 8 per group. **h** and **i** Quantification of serum cTnI and CK-MB, respectively. n = 10 per group; *$p < 0.05$ vs Sham, #$p < 0.05$ vs CME, &$p < 0.05$ vs miR-NC. **j** Western blots for Bax, Cleaved-caspase9, Cleaved-caspase3, Bcl-2 and GAPDH in protein extracted from Sham, CME, miR-NC, miR-mimic group rat hearts. n = 4 per group. **k** Relative quantification of Western-blots in j. n = 4 per group; *$p < 0.05$ vs Sham, #$p < 0.05$ vs CME, &$p < 0.05$ vs miR-NC (colour figure online)

Table 1 Cardiac function measure by echocardiography

Group	n	LVEF(%)	LVEDd	LVEDs	LVFS
Sham	8	89.96 ± 2.33	4.80 ± 0.72	2.14 ± 0.33	55.85 ± 3.48
CME	8	50.86 ± 11.91*	6.44 ± 0.58*	4.98 ± 0.83*	22.81 ± 6.69*
miR-NC	8	55.05 ± 12.63*	6.64 ± 0.71*	4.96 ± 0.93*	25.35 ± 7.30*
miR-mimic	8	83.36 ± 2.94*#&	5.70 ± 0.26*#&	2.93 ± 0.42*#&	47.13 ± 3.25*#&
miR-inhibitor	8	53.29 ± 1.96[a]	7.03 ± 0.33[a]	5.33 ± 0.30[a]	24 ± 1.24[a]

LVEF left ventricular ejection fraction, *LVEDd* left ventricular end-diastolic diameter, *LVEDs* left ventricular end-systolic diameter, *LVFS* left ventricular fractional shortening

*$p < 0.05$ versus Sham, #$p < 0.05$ versus CME, &$p < 0.05$ versus miR-NC, [a]$p < 0.05$ versus miR-mimic

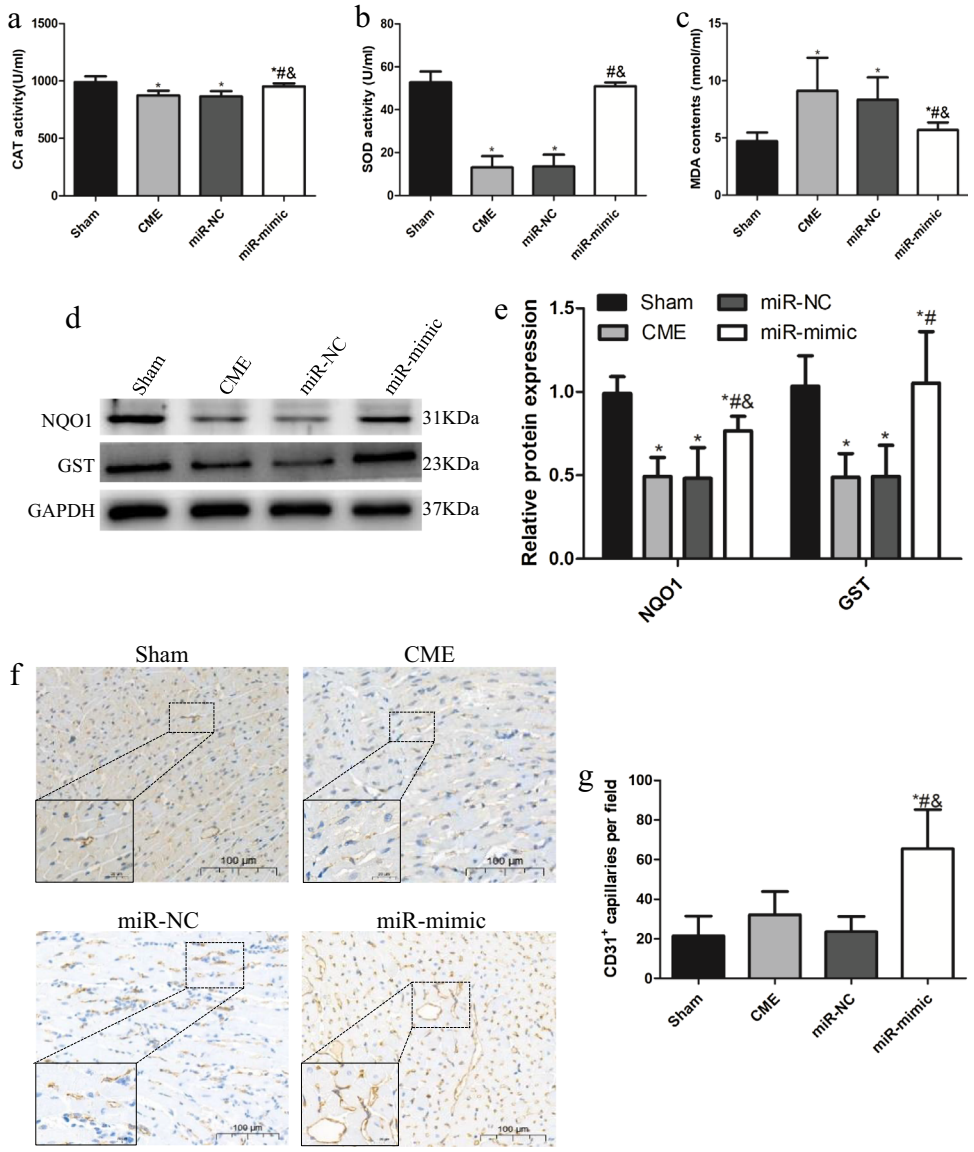

Fig. 3 In vivo delivery of miR-29b-3p improved myocardial antioxidative ability after CME and promotes neovascularization. **a** through **c** ELISA essays detecting the concentration or activity of serum CAT, SOD and MDA. n = 10 per group; *$p < 0.05$ vs Sham, #$p < 0.05$ vs CME, &$p < 0.05$ vs miR-NC. **d** Western blots for antioxidative protein NQO1 and GST. n = 5 per group. **e** Quantification of expression levels of NQO1 and GST, and GAPDH served as an internal control. n = 5 per group; *$p < 0.05$ vs Sham, #$p < 0.05$ vs CME, &$p < 0.05$ vs miR-NC. **f** Capillaries densities evaluated by immunohistochemistry analysis of CD31 in the heart section of Sham, CME, miR-NC and miR-mimic groups. n = 6 per group, scale bar = 100 μm. **g** Quantitative analysis of $CD31^+$ vessel density in Sham, CME, miR-NC and miR-mimic heart sections. n = 18 fields pooled from the analysis of 6 rat. *$p < 0.05$ vs Sham, #$p < 0.05$ vs CME, &$p < 0.05$ vs miR-NC

Pre-treatment with miR-29b-3p mimic promotes myocardial angiogenesis

It was reported that miR-29b-3p is necessary for normal endothelial function in human and rat vessels, miR-29b-3p mimic treatment can restore normal endothelium-dependent vasodilation [17]. In addition, several studies have revealed that miR-29b-3p can improve recovery in animal models of femoral fracture and spinal cord injury, and the underlying mechanism was related to miR-29b-3p promoting

angiogenesis. [18, 19]. Thus, we speculated that pre-treatment with miR-29b-3p mimic alleviates myocardial injury may be related to the property of miR-29b-3p promote neovascularization. To determine whether miR-29b-3p mimic pre-treatment could promote angiogenesis in rat myocardial, we performed myocardium CD31 immunohistochemistry staining to assess neovascularization. We found a markedly increased $CD31^+$ stained vessel density in rats pretreated with miR-29b-3p mimic compared with the sham, CME, and miR-NC groups (Fig. 3f, g). This result suggested that increased angiogenesis during miR-29b-3p upregulation, inducing myocardial protective effect.

miR-29b-3p directly targets BMF and GSK-3β for repression

Because miR-29b-3p inhibited myocardial apoptosis and promote angiogenesis, we looked for direct downstream effector by which miR-29b-3p exerts its function. Based on the predicted score of binding site, we found that BMF and GSK-3β was correlated to apoptosis and angiogenesis respectively, and both of which are strong candidates target of miR-29b-3p. As shown in Fig. 4a, the predicted target BMF and GSK-3β contains a putative miR-29b-3p binding site in their 3′UTR. Additionally, dual luciferase reporter assay results revealed that miR-29b-3p mimic significantly suppressed the relative luciferase activity in the HEK-293 T cells transfected with the BMF 3'UTR-wt or GSK-3β 3′UTR-wt, while the luciferase activity in the 293 T cells transfection with BMF 3'UTR-mut or GSK-3β 3′UTR-mut was unchanged (Fig. 4b, c). What's more, the direct target genes BMF and GSK-3β protein expression level were significantly inhibited by miR-29b-3p mimic transfection compared with the CME and miR-NC groups (Fig. 4d, e). These results demonstrated that miR-29b-3p directly target BMF and GSK-3β for repression.

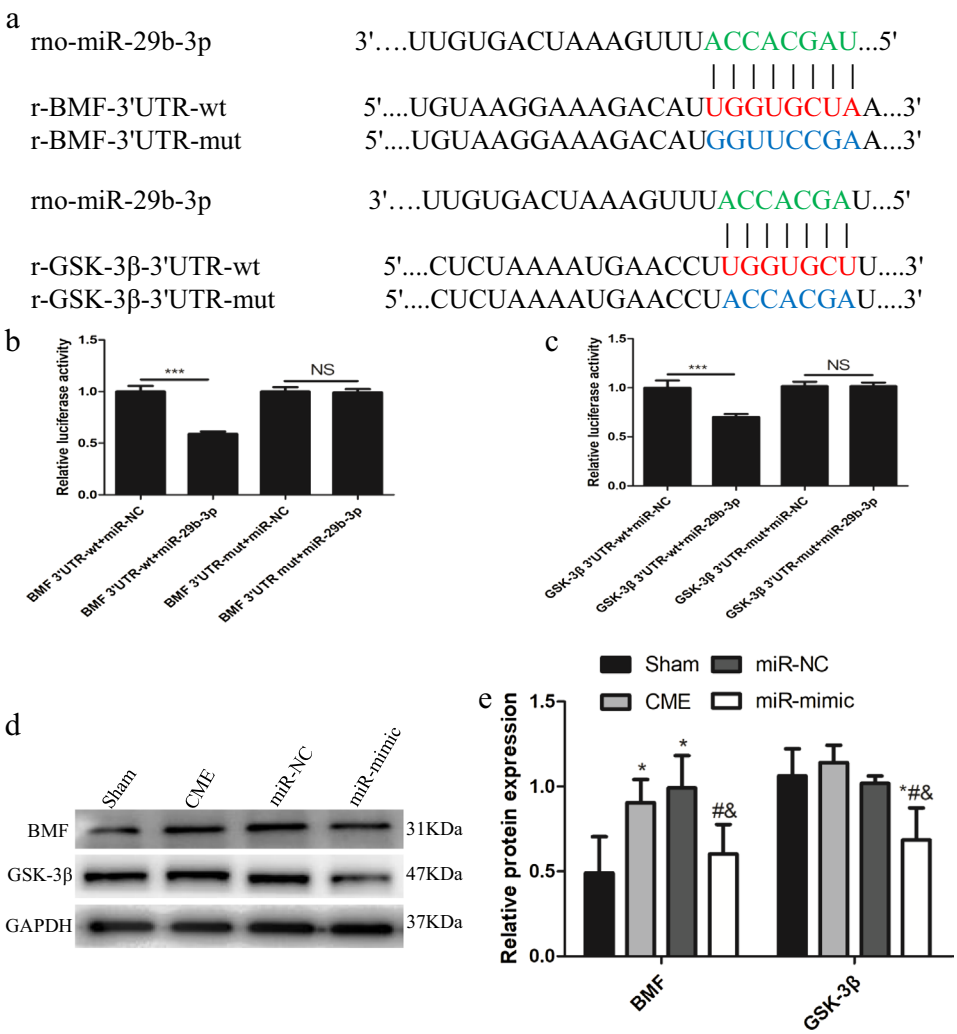

Fig. 4 miR-29b-3p directly targets the 3′UTR of BMF and GSK-3β for repression. **a** The predicted binding site of miR-29b-3p with BMF and GSK-3β. Base pairs highlighted in colors are seed sequences that are complimentary between miRNA and targets (miR-29b-3p in green and target genes 3′UTR in red). Mutations in miR-29b3p binding sites for luciferase assay in 3′UTR are indicated in blue. **b** and **c** miR-29b3p regulated the luciferase activity of plasmids that carried BMF 3′UTR-wt and GSK3β 3′UTR-wt rather than BMF 3′UTR-mut and GSK-3β 3′UTR-mut (wt, wild type; mut, mutant type) in HEK-293 T cells. n = 3 per group; ***$p < 0.05$ vs miR-NC. **d** and **e.** Western blot comparing protein expression levels of BMF and GSK-3β among Sham, CME, miR-NC, miR-mimic groups. n = 6 per group; *$p < 0.05$ vs Sham, #$p < 0.05$ vs CME, &$p < 0.05$ vs miR-NC (colour figure online)

miR-29b-3p inhibition aggravates CME-induced myocardial apoptosis and injury

To further investigate the regulatory relationship among miR-29b-3p, BMF and GSK-3β, we perform loss of function experiments of miR-29b-3p through inhibiting endogenous miR-29b-3p expression via tail vein injection of AAV9-miR-29b-3p inhibitor complex with lipofectamine mediated 28 days ahead of CME modeling in rat. As shown in the Fig. 5a, miR-29b-3p expression level was significantly declined after miR-inhibitor transfection. Meanwhile, inhibition of miR-29b-3p resulted in declined cardiac function (Fig. 5b and Table 1), reduced neovascularization (Fig. 5c, d), increased myocardial apoptosis (Fig. 5e, f), increased myocardial microinfarct sizes (Fig. 5g, h), increased expression of target genes BMF and GSK-3β, and increased pro-apoptotic protein expression compared with miR-mimic (Fig. 5i, j). The aforementioned findings further showed that in vivo overexpression of miR-29b-3p in a rat CME model reduced myocardial microinfarct size, reduced cardiac dysfunction, and enhanced myocardial angiogenesis. Suppression of BMF and GSK-3β was partially responsible for these protective effects.

Discussion

In the current study, we discovered a new role for miR-29b-3p in the regulation of myocardial apoptosis and cardiac angiogenesis. We demonstrated that miR-29b-3p down-regulated 12 h after CME modeling, pre-treatment with AAV9-miR-29b-3p mimics 28 days before CME surgery can significant increase myocardium miR-29b-3p expression level, which inhibits cardiomyocytes apoptosis, reduces myocardial microinfarct size, attenuates cardiac dysfunction and promotes myocardial neovascularization. In addition, we identified BMF and GSK-3β as the direct targets of miR-29b-3p, in which BMF is positive correlate with apoptosis, while GSK-3β is negatively regulates angiogenesis. Finally, we transfected rat with AAV9-miR-29b-3p inhibitors, and found that reduction of miR-29b-3p enhanced myocardial apoptosis and impaired heart function post-CME. Thus, our results reveals an important function of the miR-29b-3p in CME-induced myocardial injury.

CME can lead to progressive cardiac contractile dysfunction, myocardium microinfarcts, cardimyocytes apoptosis and reduced coronary blood flow reserve [1]. The incidence of CME is a strong predictor of worse prognosis in patients with CAD, which independence to myocardial infarct size [20]. In clinical CME treatment, no matter protection devices or antiplatelet drugs it is, the effect is modest of best. Therefore, develop novel therapeutic strategies is urgently needed. Studies has revealed that after myocardial injury, changes in the non-coding RNA transcriptome implicate in the pathophysiology process of cardiovascular disease [21–23]. The dynamic expression of non-coding RNA plays a vital role in adjusting the occurrence and development of diseases. By detecting miR-29b-3p expression level in myocardium 12 h after CME modeling, we discovered that miR-29b-3p was remarkably reduced in CME rat heart tissues, which was positive correlated with the impair cardiac function, larger microinfarct areas and elevated TUNEL-positive cardiomyocytes. Interestingly, when miR-29b-3p was upregulated in rat heart tissues, we found a decreased myocardial apoptosis, reduced microinfarct size, improved cardiac function and promoted angiogenesis. In contrast, the down-regulated of miR-29b-3p in the myocardium exert reversely effects. Accordingly, our findings indicate that the upregulation of miR-29b-3p play a myocardial protective role in reduce CME-induced myocardial injury.

To further study the underlying mechanism by which miR-29b-3p reduce myocardial apoptosis and promote neovascularization, we search for target genes which was related to apoptosis and angiogenesis regulation. By using bioinformatics analysis and literatures review, we find that BMF and GSK-3β were the targets of miR-29b-3p with high possibility. BMF, a pro-apoptotic BCL-2 homology 3 (BH3)-only member of the B-cell lymphoma 2 (Bcl-2) family, which contains a short BH3 domain and its BH3 domain is required both for binding to prosurvival Bcl-2 proteins and for triggering intrinsic apoptosis [24]. Apoptosis is necessary for mammals to maintain physiological equilibrium. However, calamity can result when the tissue apoptosis process goes wrong. Studies have demonstrated that the imbalance of Bcl-2 family proteins are the key factor to induce overwhelm apoptosis and result in disease [25]. When damage signals continuous stimulate, BMF secret increase and bind to prosurvival Bcl-2 family proteins, which induce antiapoptotic protein degradation and cause excessive apoptosis [26]. Consistence with this, we found BMF expression level was significantly increased in the CME and miR-NC group, together with Cleaved-caspase3, Cleaved-caspase9 and Bax elevated, while Bcl-2 was remarkably decreased. Additionally, heart tissue sections TUNEL staining also show obviously cardiomyocytes apoptosis in this two group. Nevertheless, the expression level of proapoptotic protein and TUNEL-positive cardiomyocytes were significantly decreased in the miR-mimic group. In contrast, pretreatment rat with miR-inhibitor exert reversely effects compared with the miR-mimic group. GSK-3β, belonging to the highly conserved glycogen synthase kinase subfamily, implicating in numerous cellular processes including cell proliferation, apoptosis and angiogenesis. Previous studies have demonstrated the helpful role of inhibiting GSK-3β for neovascularization and improves angio-architecture. Reduction of GSK-3β promotes myocardial neovascularization in rat myocardial infarction (MI)

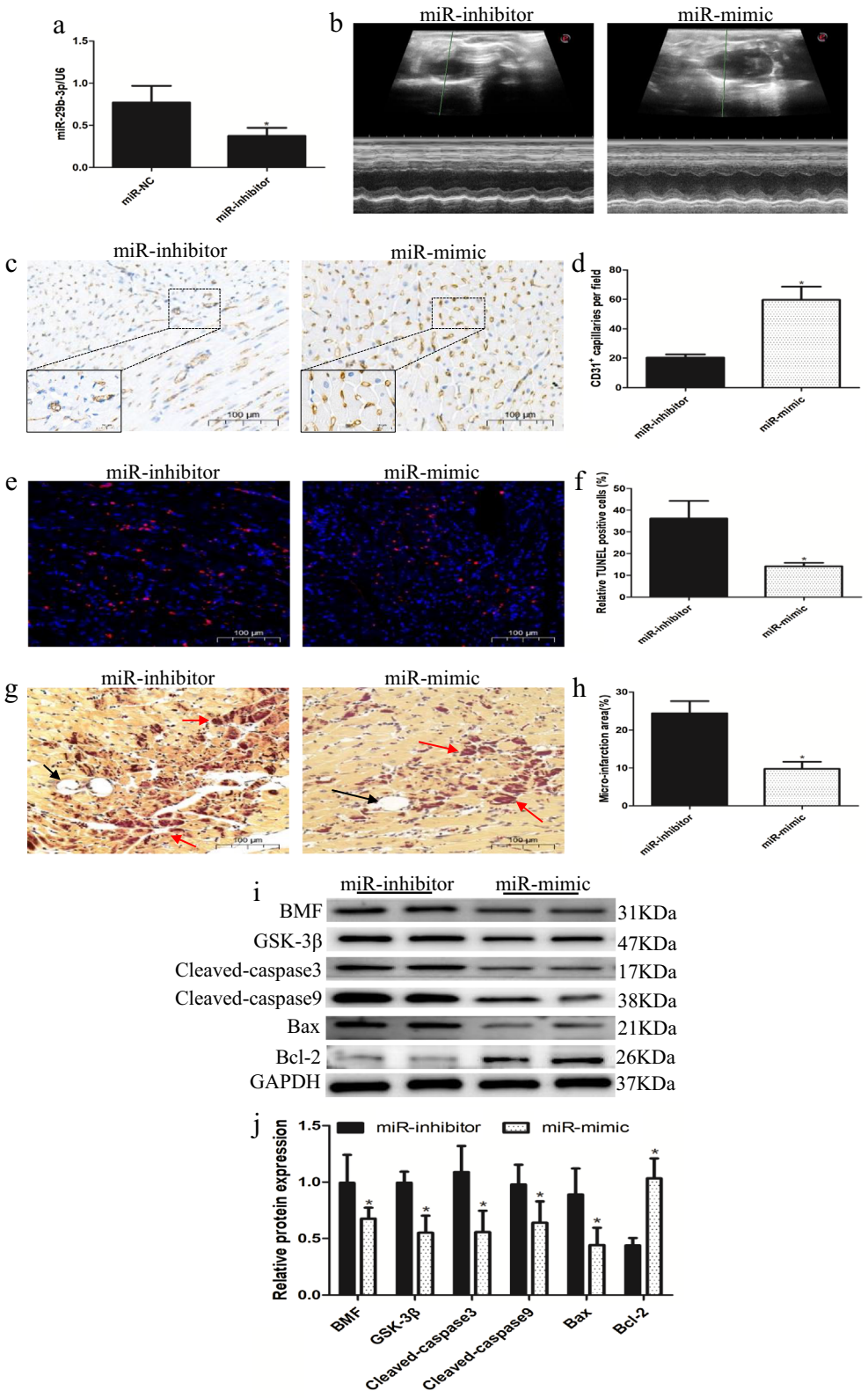

model [27]. In a chronic myocardial ischemia pig model, inhibition of GSK-3β significant promote angiogenesis and blood flow reserve in ischemia myocardium [28]. Similarly, Senger et al. showed that inhibition of GSK-3β improved vascular cord formation and promoted neovessel formation both in vitro and in vivo [29]. What's more, a recent

◂**Fig. 5** In vivo delivery of miR-29b-3p inhibitor exert inversely effects compared with the miR-mimic group. **a** Relative miR-29b-3p expression level was decreased in miR-inhibitor treated rats. n = 8 per group; ***$p < 0.05$ vs miR-NC. **b** M-mode echocardiography of representative hearts 12 h after CME in miR-inhibitor and miRmimic treated rat. n = 8 per group. **c.** Immunohistochemistry analysis of $CD31^+$ for detecting angiogenesis in miR-inhibitor and miR-mimic transfected heart sections. n = 6 per group, scale bar = 100 μm. **d** Quantification of the capillaries density in miR-inhibitor and miR-mimic transfected heart sections. n = 18 fields per group; *$p < 0.05$ vs miR-inhibitor. **e** Myocardial apoptosis evaluated by TUNEL staining in miR-inhibitor and miR-mimic transfected heart sections. n = 6 per group, scale bar = 100 μm. **f** Quantitative analysis of TUNEL-positive cardiomyocytes in miR-inhibitor and miR-mimic treated rat heart sections. n = 6 per group; *$p < 0.05$ vs miR-inhibitor. **g** Myocardial microinfarct foci evaluated by HBFP staining in miR-inhibitor and miR-mimic transfected heart sections. The black arrow indicates microspheres, red arrow shows myocardial microinfarct foci. n = 5 per group, scale bar = 100 μm. **h** Quantitative analysis of microinfarct areas in miR-inhibitor and miR-mimic treated rat heart sections. n = 5 per group; *$p < 0.05$ vs miR-inhibitor. **i** Western blots analysis of target genes and apoptosis related protein expression level in miR-inhibitor and miR-mimic treated rat myocardium. n = 6 per group. **j** Relative quantification of BMF, GSK-3β, Cleavedcaspase3, Cleaved-caspase9, Bax and Bcl-2 expression level. GAPDH was used as an internal control. n = 6 per group; *$p < 0.05$ vs miR-inhibitor (colour figure online)

work found that circNfix downregulation increased miR-214 expression level, which promoted myocardial angiogenesis via inhibiting GSK-3β in a mice MI model [30]. Consistent with this, we found the expression of GSK-3β was decreased in CME rat with miR-29b-3p mimics transfected, and myocardial capillary density remarkably increased. However, the expression level of GSK-3β and vessel density were no significant difference among sham, CME and miR-NC groups. For bioinformatics analysis, we query through the miRNAs database, and validate the analysis results via dual luciferase reporter assay. As our expected, transfected with miR-29b-3p mimics significantly decreased the relative luciferase activity of the BMF 3′UTR-wt and GSK-3β 3′UTR-wt, but did not change the luciferase activity of the vector containing BMF 3'UTR-mut and GSK-3β 3′UTR-mut. These data suggest miR-29b-3p directly target BMF and GSK-3β for repression, inhibiting myocardial apoptosis and promote myocardium neovascularization.

The mature miR-29 s member are highly conserved among humans, mice, and rats, sharing the same seed sequences region [31]. Increasing studies shows that miR-29b-3p has distinct expression profiles and play different roles in various cardiovascular disease. In a mouse MI model, researchers discovered that upregulation of miR-29b-3p can significant alleviated MI-induced cardiac fibrosis and attenuated myocardial remodeling post-MI [12]. Peng found that upregulation of miR-29b-3p significant reduced cardiomyocytes apoptosis and myocardial inflammation in endotoxin-induced cardiac injury [32]. Numerous growth factors have been shown to be associated with neovascularization and angio-architecture, but little is understood about the complex mechanisms governing upstream control of gene translation and expression. Endothelial cells have a high concentration of miR-29 s, which suggests that miR-29 s are crucial for maintaining vascular integrity, according to a miRNAs array [33–35]. Our study data suggest that transfected with miR-29b-3p 28 days before CME operation can significant promotes myocardium angiogenesis, mechanistic analysis revealed this effect may be obtain by inhibiting GSK-3β. It is important to highlight that mounting data suggests that miR-29b-3p operates differently under diverse pathological conditions. Upregulating miR-29b-3p is a successful strategy to reduce myocardial fibrosis in a mouse model of MI caused by a blocked left coronary artery [12]. However, in a mouse model of ventricular pressure overload, miR-29b global genetic deletion or antimiR-29 infusion reduce cardiac hypertrophy and fibrosis and improve cardiac function [36]. Depending on the experimental setup and the time points analyzed the endogenous expression levels of miR-29b-3p appear to differ. To identify the specific roles of miR-29b-3p, a more thorough analysis of miR-29 expression in various cell types, organs, and disease models may be fruitful.

There are two limitations to this study. First, we established that the chronic upregulation of miR-29b-3p facilitated myocardial angiogenesis; nevertheless, the mechanisms between high levels of miR-29b-3p and neovascularization in the adult rat heart requires more investigation. Second, considering that miR-29b-3p has numerous targets, while we only mentioned two of them. Given the pleiotropic effects of miRNAs, prospective treatment approaches based on miR-29b-3p overexpression demand careful thought.

In conclusion, the current findings showed that miR-29b-3p is decreased in CME-induced myocardial injury. By inhibiting the synthesis of BMF and GSK-3β, miR-29b-3p upregulation enhances cardiac function and prevents myocardial apoptosis. Therefore, miR-29b-3p overexpression may be helpful in treating cardiac problems brought on by CME.

Author contributions LL and XW conceived the project and designed experiments. ZQ, XW, YZ, JZ and HL performed the experiments. ZQ and XW analyzed the data. ZQ and LL wrote the manuscript.

Funding This work was supported from the Project for Innovative Research Team in Guangxi Natural Science Foundation (No. 2018GXNSFGA281006), National Nature Science Foundation of China (No. 82170349, No. 81900318), and Guangxi Natural Science Foundation (No. 2018GXNSFBA050017).

Data availability The datasets used or analyzed during the current study are available from the corresponding author on reasonable request.

Declarations

Conflict of interest The authors declare there are no conflicts of interest.

References

1. Kleinbongard P, Heusch G (2022) A fresh look at coronary microembolization. Nat Rev Cardiol 19(4):265–280
2. Skyschally A, Walter B, Heusch G (2013) Coronary microembolization during early reperfusion: infarct extension, but protection by ischaemic postconditioning. Eur Heart J 34(42):3314–3321
3. Taqueti VR, Solomon SD, Shah AM et al (2018) Coronary microvascular dysfunction and future risk of heart failure with preserved ejection fraction. Eur Heart J 39(10):840–849
4. Heusch G (2020) Myocardial ischaemia-reperfusion injury and cardioprotection in perspective. Nat Rev Cardiol 17(12):773–789
5. de Waha S, Patel MR, Granger CB et al (2017) Relationship between microvascular obstruction and adverse events following primary percutaneous coronary intervention for ST-segment elevation myocardial infarction: an individual patient data pooled analysis from seven randomized trials. Eur Heart J 38(47):3502–3510
6. Su Q, Lv X, Sun Y et al (2018) Role of TLR4/MyD88/NF-κB signaling pathway in coronary microembolization-induced myocardial injury prevented and treated with nicorandil. Biomed Pharmacother 106:776–784
7. Qin Z, Kong B, Zheng J et al (2020) Alprostadil injection attenuates coronary microembolization-induced myocardial injury through GSK-3β/Nrf2/HO-1 signaling-mediated apoptosis inhibition. Drug Des Devel Ther 14:4407–4422
8. Jonas S, Izaurralde E (2015) Towards a molecular understanding of microRNA-mediated gene silencing. Nat Rev Genet 16(7):421–433
9. Ha M, Kim VN (2014) Regulation of microRNA biogenesis. Nat Rev Mol Cell Biol 15(8):509–524
10. Zhou SS, Jin JP, Wang JQ et al (2018) miRNAS in cardiovascular diseases: potential biomarkers, therapeutic targets and challenges. Acta Pharmacol Sin 39(7):1073–1084
11. Liu MN, Luo G, Gao WJ et al (2021) miR-29 family: a potential therapeutic target for cardiovascular disease. Pharmacol Res 166:105510
12. van Rooij E, Sutherland LB, Thatcher JE et al (2008) Dysregulation of microRNAs after myocardial infarction reveals a role of miR-29 in cardiac fibrosis. Proc Natl Acad Sci U S A 105(35):13027–13032
13. Marques FZ, Vizi D, Khammy O et al (2016) The transcardiac gradient of cardio-microRNAs in the failing heart. Eur J Heart Fail 18(8):1000–1008
14. Cai Y, Li Y (2019) Upregulation of miR-29b-3p protects cardiomyocytes from hypoxia-induced apoptosis by targeting TRAF5. Cell Mol Biol Lett 24:27
15. Li L, Zhao X, Lu Y et al (2010) Altered expression of pro- and anti-inflammatory cytokines is associated with reduced cardiac function in rats following coronary microembolization. Mol Cell Biochem 342(1–2):183–190
16. Weidner N, Folkman J, Pozza F et al (1992) Tumor angiogenesis: a new significant and independent prognostic indicator in early-stage breast carcinoma. J Natl Cancer Inst 84(24):1875–1887
17. Widlansky ME, Jensen DM, Wang J et al (2018) miR-29 contributes to normal endothelial function and can restore it in cardiometabolic disorders. EMBO Mol Med 10(3):e8046
18. Yang J, Gao J, Gao F et al (2022) Extracellular vesicles-encapsulated microRNA-29b-3p from bone marrow-derived mesenchymal stem cells promotes fracture healing via modulation of the PTEN/PI3K/AKT axis. Exp Cell Res 412(2):113026
19. Xiao X, Li W, Rong D et al (2021) Human umbilical cord mesenchymal stem cells-derived extracellular vesicles facilitate the repair of spinal cord injury via the miR-29b-3p/PTEN/Akt/mTOR axis. Cell Death Discov 7(1):212
20. Heusch G, Kleinbongard P, Böse D et al (2009) Coronary microembolization: from bedside to bench and back to bedside. Circulation 120(18):1822–1836
21. Lu D, Thum T (2019) RNA-based diagnostic and therapeutic strategies for cardiovascular disease. Nat Rev Cardiol 16(11):661–674
22. Small EM, Frost RJ, Olson EN (2010) MicroRNAs add a new dimension to cardiovascular disease. Circulation 121(8):1022–1032
23. Zhu L, Li N, Sun L et al (2021) Non-coding RNAs: the key detectors and regulators in cardiovascular disease. Genomics 113(1 Pt 2):1233–1246
24. Puthalakath H, Villunger A, O'Reilly LA et al (2001) Bmf: a proapoptotic BH3-only protein regulated by interaction with the myosin V actin motor complex, activated by anoikis. Science 293(5536):1829–1832
25. Singh R, Letai A, Sarosiek K (2019) Regulation of apoptosis in health and disease: the balancing act of BCL-2 family proteins. Nat Rev Mol Cell Biol 20(3):175–193
26. Banjara S, Suraweera CD, Hinds MG et al (2020) The Bcl-2 family: ancient origins, conserved structures, and divergent mechanisms. Biomolecules 10(1):128
27. Kaga S, Zhan L, Altaf E et al (2006) Glycogen synthase kinase-3beta/beta-catenin promotes angiogenic and anti-apoptotic signaling through the induction of VEGF, Bcl-2 and survivin expression in rat ischemic preconditioned myocardium. J Mol Cell Cardiol 40(1):138–147
28. Potz BA, Sabe AA, Elmadhun NY et al (2016) Glycogen synthase kinase 3β inhibition improves myocardial angiogenesis and perfusion in a swine model of metabolic syndrome. J Am Heart Assoc 5(7):e003694
29. Hoang MV, Nagy JA, Senger DR (2011) Cdc42-mediated inhibition of GSK-3β improves angio-architecture and lumen formation during VEGF-driven pathological angiogenesis. Microvasc Res 81(1):34–43
30. Huang S, Li X, Zheng H et al (2019) Loss of super-enhancer-regulated circRNA Nfix induces cardiac regeneration after myocardial infarction in adult mice. Circulation 139(25):2857–2876
31. Kriegel AJ, Liu Y, Fang Y et al (2012) The miR-29 family: genomics, cell biology, and relevance to renal and cardiovascular injury. Physiol Genomics 44:237–244
32. Li Z, Yi N, Chen R et al (2020) miR-29b-3p protects cardiomyocytes against endotoxin-induced apoptosis and inflammatory response through targeting FOXO3A. Cell Signal 74:109716
33. Suárez Y, Fernández-Hernando C et al (2007) Dicer dependent microRNAs regulate gene expression and functions in human endothelial cells. Circ Res 100(8):1164–1173
34. Poliseno L, Tuccoli A, Mariani L et al (2006) MicroRNAs modulate the angiogenic properties of HUVECs. Blood 108(9):3068–3071
35. Urbich C, Kuehbacher A, Dimmeler S (2008) Role of microRNAs in vascular diseases, inflammation, and angiogenesis. Cardiovasc Res 79(4):581–588
36. Sassi Y, Avramopoulos P, Ramanujam D et al (2017) Cardiac myocyte miR-29 promotes pathological remodeling of the heart by activating Wnt signaling. Nat Commun 8(1):1614